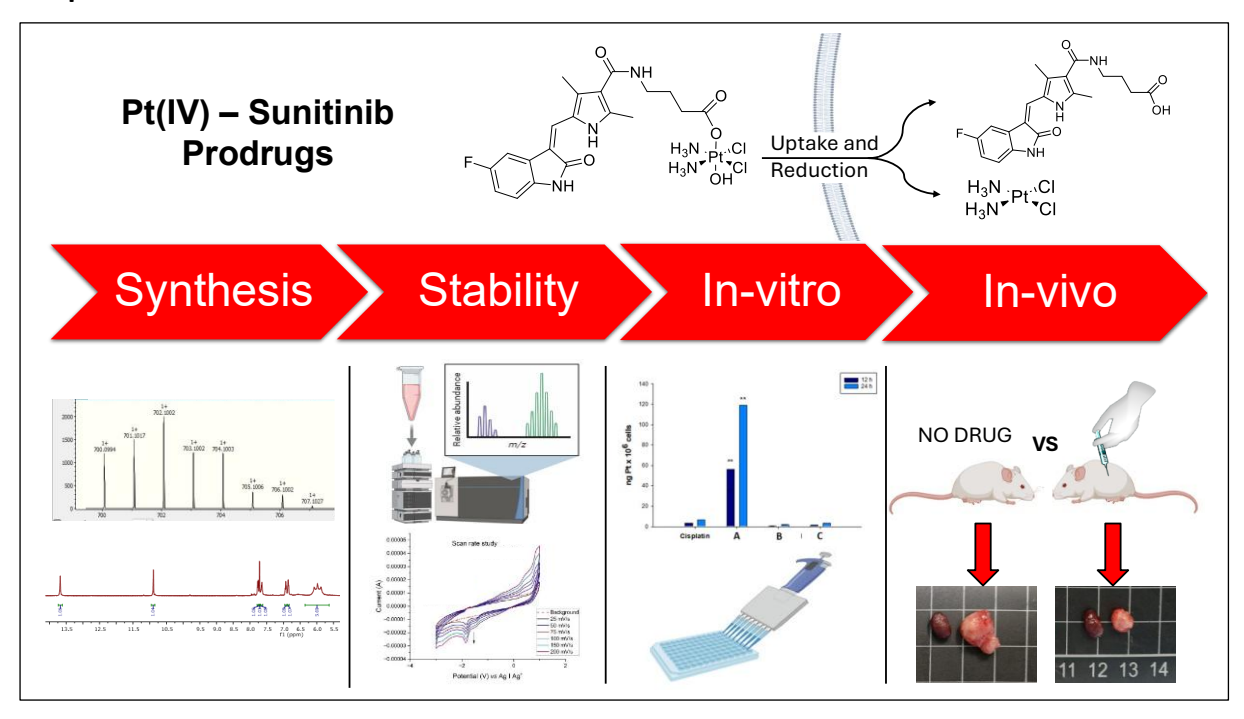
# Sunitinib-derived Pt(IV) complexes display enhanced anticancer activity against renal cell carcinoma compared to conventional platinum chemotherapy

Darren F. Beirne<sup>1</sup>, Jemma Arakelyan<sup>2</sup>, Matteo Forner<sup>3</sup>, Ho-Jung Choe<sup>2</sup>, Eithne Dempsey<sup>1,4</sup>, Valentina Gandin<sup>3</sup>, Trinidad Velasco-Torrijos<sup>1,4</sup>, Maria V. Babak<sup>2\*</sup>, Diego Montagner<sup>1,4\*</sup>

Department of Chemistry, Maynooth University, Maynooth, Ireland
Department of Chemistry, City University of Hong Kong, Hong Kong, China SAR
Universita' di Padova, Dipartimento di Scienze del Farmaco, Padova, Italy
Kathleen Londsdale Institute for Human Health Research, Maynooth University, Ireland Corresponding authors: <a href="mailto:diego.montagner@mu.ie">diego.montagner@mu.ie</a>; <a href="mailto:mbabak@cityu.edu.hk">mbabak@cityu.edu.hk</a>

**Keywords:** Pt(IV) prodrugs, Sunitinib, Tyrosine Kinase Inhibitor (TKI), Anticancer, Dual-action, renal cell carcinoma (RCC)

# **Graphical Abstract**



## **Abstract**

Half of all cancer treatments worldwide involve the use of Pt chemotherapeutics but despite their wide clinical usage, Pt drugs have severe disadvantages, including cell toxicity. Sunitinib is a FDA approved Tyrosine Kinase Inhibitor which selectively targets renal cell carcinoma due to the overexpression of its receptors such as vascular endothelial growth factor receptor (VEGFR) and platelet derived growth factor receptor (PDGFR). Here, a family of three Pt(IV) prodrugs, based on the clinically approved cisplatin, oxaliplatin and carboplatin, bearing sunitinib-derived axial ligands have been developed with the aim to overcome healthy cell

toxicity. This study highlights the first Pt(IV) complexes targeting renal carcinoma tumours overexpressing VEGFR. Conjugation of the sunitinib-based ligand was shown not to jeopardize its kinase inhibitory activity. *In vitro* cytotoxicity proved the cisplatin prodrug derivative to be 36 times more active to cisplatin chemotherapy and 3D spheroids assays reinforced this superior activity. The cisplatin-based prodrug was tested *in vivo* against renal carcinoma xenografts, revealing exceptional superior activity to cisplatin control. This work demonstrates the excellent potential of Pt(IV)-Sunitinib conjugates for the treatment of Renal cell carcinoma, as they display far enhanced tumour reduction and lower systemic toxicity when compared to cisplatin chemotherapy.

#### Introduction

Cisplatin, oxaliplatin and carboplatin are three of the most widely used Pt(II)-based anticancer chemotherapeutics and are approved worldwide for the treatment of various cancer types, including testicular<sup>1</sup>, colorectal<sup>2</sup>, ovarian<sup>3,4</sup> and lung<sup>4</sup> cancers (**Figure 1**). Although 50% of all cancer treatments involve the use of Pt (II) drugs<sup>5</sup>, their clinical success is hindered by three main disadvantages: (i) toxic side-effects<sup>6-11</sup>, (ii) acquired/innate drug resistance<sup>12,13</sup> and/or, (iii) poor oral bioavailability<sup>14</sup>. Pt(IV) prodrugs address these limitations. As octahedral, kinetically inert d<sup>6</sup> complexes<sup>15</sup> with high stability in the bloodstream, <sup>16-20</sup> they act as prodrugs, activated *via* intracellular reduction simultaneously releasing the cytotoxic Pt(II) species and the axial ligands. Importantly, <sup>16-20</sup>many Pt(IV) prodrugs described in the literature carry at least one bioactive axial ligand<sup>21-23</sup>.

Conjugating tyrosine kinase inhibitors (TKIs) to Pt(IV) prodrugs represents a promising strategy. Tyrosine kinases catalyse the transfer of phosphate groups from adenosine triphosphate (ATP) to intracellular proteins, regulating cellular growth and proliferation<sup>24</sup>. Kinases receptors such as Vascular Endothelial Growth Factor Receptor (VEGFR) and Platelet Derived Growth Factor Receptor (PDGFR) <sup>24</sup>are frequently overexpressed in multiple cancers,<sup>25–31</sup> making TKIs like imatinib, gefitinib and dasatinib (**Figure 1**) clinically valuable for treating different tumour types. To date, four Pt(IV)-TKI conjugates have been reported: Pt(IV)-gefitinib<sup>32,33</sup>/erlotinib<sup>33</sup> derivatives, a Pt(IV)-dasatinib analogue<sup>34</sup>, and Pt(IV)-Imatinib/Nilotinib derivatives<sup>35</sup>. None of the aforementioned Pt(IV)-TKI conjugates use a TKI ligand that has clinical approval for use against VEGFR expressing tumours. We sought to develop a family of Pt(IV)-TKI complexes that target VEGFR for the treatment of renal cell carcinomas.

#### Globally Approved Pt(II) Chemotherapeutics

#### FDA and/or EU Approved Tyrosine Kinase Inhibitors

**Figure 1.** Top: Structures of three worldwide approved Pt(II) anticancer chemotherapeutics. Bottom: Structures of imatinib, sunitinib, gefitinib and dasatinib.

Sunitinib (**Figure 1**) is an FDA approved TKI that is clinically used for the treatment of renal cell carcinoma (RCC), imatinib-resistant gastrointestinal stromal tumour (GIST) and pancreatic cancer<sup>36</sup>. The combination of cisplatin and sunitinib demonstrated synergistic or additive effects against a wide range of cancer types, including gastric, urothelial, testicular, thyroid, bladder cancers, both *in vitro* and *in vivo*<sup>37–41</sup>. As such, incorporating sunitinib into a Pt(IV) prodrug is expected to potentiate the activity of both drugs against tumours overexpressing VEGFR and/or PDGFR. Additionally, such prodrugs may enhance tumour selectivity and overcome resistance due to their dual mode of action. This approach is anticipated to outperform conventional chemotherapy by ensuring concomitant intracellular release of both drugs.

Here, we report the synthesis, chemical characterization, stability studies, electrochemical behaviour, biological evaluations and *in vivo* efficacy of three Pt(IV)-sunitinib-based prodrugs (**Figure 2**).

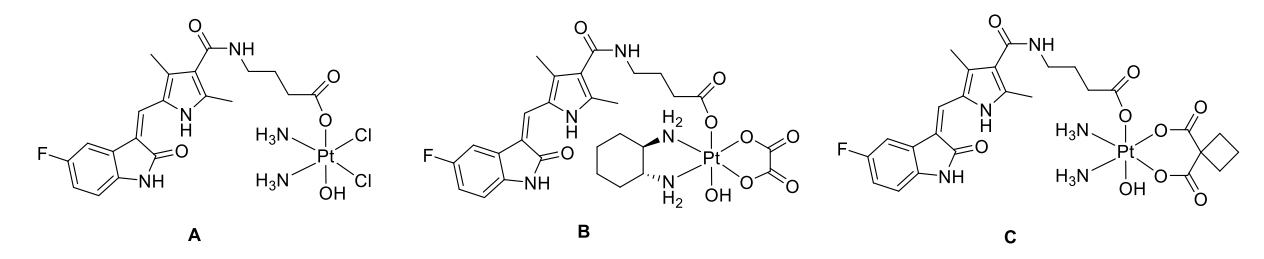


**Figure 2.** Structures of the three Pt(IV)—sunitinib prodrugs based on cisplatin (**A**), oxaliplatin (**B**) and carboplatin (**C**) pharmacophores.

# **Experimental**

Detailed material and methods and all the spectra are reported in the ESI.

# **Syntheses**

Cisplatin, dihydroxycisplatin (oxoplatin), oxaliplatin, dihydroxyoxaliplatin, carboplatin and dihydroxycarboplatin were synthesized as previously described<sup>42–44</sup>.

(Z)-5-((5-fluoro-2-oxoindolin-3-ylidene)methyl)-2,4-dimethyl-1H-pyrrole-3- carboxylic acid. (2) 1.2 g (7.65 mmol, 1 eq.) of 5-fluoro-1,3-dihydroindol-2-one and 1.47 g of 5-formyldimethyl-1H-pyrrole-3-carboxylic acid (9.6 mmol, 1.25 eq.) were added to a 250 ml round bottom flask. 60 ml of absolute EtOH was added and the mixture was stirred for 5 minutes. 12 drops of piperidine were added and the mixture was stirred at reflux for 3 hours (TLC, CHCl<sub>3</sub>:MeOH = 95:5). The mixture was allowed cool to 25°C and the solids were collected via vacuum filtration. The solid was again stirred in 22.5 ml of EtOH at 72 °C for 30 mins. The mixture was allowed cool to 25°C and the solids were collected via vacuum filtration, washed with 2 x 12 ml of EtOH and dried using a Schlenk line (yield: 1.93 g, 84%). The procedure use was adapted from a literature procedure by Sansook, et al., 2017<sup>45</sup>. <sup>1</sup>H NMR (500 MHz, DMSO):  $\delta$  13.88 (s, 1H, pyrrole-NH), 10.95 (s, 1H, indole-NH), 7.80 (dd, J = 9.4, 2.5 Hz, 1H, ArH), 7.76 (s, 1H, alkeneH), 7.00 - 6.91 (m, 1H, ArH), 6.86 (dd, J = 8.4, 4.5 Hz, 1H, ArH), 2.55 (s, 3H, CH<sub>3</sub>). <sup>13</sup>C NMR (126 MHz, DMSO-d<sup>6</sup>): 170.0, 166.4, 157.8 (J = 234.4 Hz), 141.3, 135.2, 133.9, 127.4 (J = 9.5 Hz), 126.5, 125.3, 116.1 (J = 3.4 Hz), 114.8, 113.3 (J = 23.9 Hz), 113.1, 110.6 (J = 3.4 Hz) 8.6 Hz), 110.56, 106.8 (J = 25.8 Hz), 14.9, 11.9. <sup>19</sup>F-{<sup>1</sup>H} NMR (470 MHz, CDCl<sub>3</sub>):  $\delta$  -122.371 (s, 1F). IR (ATR): 2819, 1652, 1537, 1474, 1297, 1127, 922, 759 cm<sup>-1</sup>. LC-MS: 93.4%. HRMS: Calculated mass for M: 300.0910. Found (M): 300.0913. Difference 0.93 ppm (71.59% IMS)

**methyl** (*Z*)-4-(5-((5-fluoro-2-oxoindolin-3-ylidene)methyl)-2,4-dimethyl-1*H*-pyrrole-3-carboxamido)butanoate (3). 1 g (3.3 mmol, 1 eq.) of acid derivative and 2.13 g of TBTU (6.6 mmol, 2 equivalents) were added to a round bottom flask. The flask was purged with N<sub>2</sub>, prior to addition of 20 ml of DMF followed by 2.7 ml (2.02 g, 19.9 mmol, 6 eq.) of TEA. The solution was now stirred for 20 minutes, prior to cannula addition of 1.0 g (6.6 mmol, 2 eq.) of γ-aminobutyric methyl ester dissolved in 4 mL of anhydrous DMF. The solution was stirred at room temperature for 24 hours (TLC, CHCl<sub>3</sub>:MeOH = 9:1). The solvent was removed *in vacuo* at 60°C. 300 ml of H<sub>2</sub>O was added to the residue followed by 100 ml of saturated sodium bicarbonate aqueous solution. The resulting precipitate was collected via vacuum filtration, washed with 40 ml of deionised and then dried using a Schlenk line (yield: 0.54 g, 41%). <sup>1</sup>H NMR (500 MHz, DMSO): δ 13.68 (s, 1H, pyrrole-NH), 10.90 (s, 1H, indole-NH), 7.77 (dd, *J* = 9.4, 2.5 Hz, 1H, ArH), 7.72 (s, 1H, alkeneH), 7.68 (t, *J* = 5.7 Hz, 1H, amide-NH), 6.96 – 6.90 (m, 1H,

ArH), 6.85 (dd, J = 8.4, 4.5 Hz, 1H, ArH), 3.61 (s, 3H, O-CH<sub>3</sub>), 3.25 (dd, J = 12.8, 6.8 Hz, 2H, CH<sub>2</sub>), 2.43 (s, 3H, CH<sub>3</sub>), 2.42 – 2.38 (m, 5H, CH<sub>3</sub>/CH<sub>2</sub>), 1.78 (p, J = 7.2 Hz, 2H, CH<sub>2</sub>). <sup>13</sup>C NMR (126 MHz, DMSO-d<sup>6</sup>): 173.6, 170.0, 165.2, 158.6 (d, J = 234.1 Hz) 136.8, 134.9, 130.7, 127.5 (d, J = 9.4 Hz), 126.2, 125.3, 121.4, 115.0 (d, J = 6.6 Hz), 112.9 (d, J = 21.2 Hz), 112.5, 112.4, 110.4 (d, J = 8.7 Hz), 106.5, 106.3 (d, J = 28.1 Hz), 51.7, 38.5, 31.3, 25.1, 13.1, 10.9. <sup>19</sup>F-{<sup>1</sup>H} NMR (470 MHz, DMSO): δ -122.56 (s, 1F). IR (ATR): 3292, 2952, 1730, 1621, 1538, 1475, 1376, 1194, 1161, 922, 860, 793, 696, 607, 446 cm<sup>-1</sup>. LC-MS: Calculated mass for (M+H)<sup>+</sup>: 400, Found: 400.4 (100%). HRMS: Calculated mass for M: 399.1594. Found (M): 399.1601. Difference 1.66 ppm (95.78% IMS).

Synthesis of (Z)-4-(5-((5-fluoro-2-oxoindolin-3-ylidene)methyl)-2,4-dimethyl-1H-pyrrole-3carboxamido)butanoic acid (4). 0.52 g (1.3 mmol, 1 eq.) of ester derivative was suspended in 60 ml of MeOH. 10 mL of 5 M NaOH was added and the mixture was sonicated for 5 minutes. The mixture was stirred at room temperature for 2 hours (TLC, CHCl<sub>3</sub>:MeOH = 9:1). The MeOH was removed in vacuo. 1 M HCl was added to the aqueous mixture until the mixture was acidified to pH = 4. The precipitate was collected via vacuum filtration, washed with abundant  $H_2O$  and dried using a Schlenk line (yield: 0.44 g, 86%). <sup>1</sup>H NMR (500 MHz, DMSO):  $\delta$  13.68 (s, 1H, pyrrole-NH), 12.09 (s, 1H, COOH), 10.89 (s, 1H, indole-NH), 7.77 (dd, J = 8.6 Hz, 1H, ArH), 7.72 (s, 1H, alkene-H), 7.67 (t, 1H, amide-NH), 6.93 (t, J = 8.1 Hz, 1H, ArH), 6.85 (dd, J = 8.0, 4.4 Hz, 1H, ArH), 3.25 (d, J = 6.0 Hz, 2H, CH<sub>2</sub>), 2.44 (s, 3H, pyrrole-CH<sub>3</sub>), 2.42 (s, 3H, pyrrole-CH<sub>3</sub>), 2.30 (t, J = 7.2 Hz, 2H, CH<sub>2</sub>), 1.78 – 1.71 (m, 2H, CH<sub>2</sub>). <sup>13</sup>C NMR (126 MHz, DMSO-d<sup>6</sup>):  $\delta$ 174.7, 170.0, 165.2, 158.2 (d, J = 234.1 Hz), 157.7, 136.8, 134.97, 130.7, 127.6 (d, J = 9.6 Hz), 126.2, 125.3, 121.5, 114.9 (d, J = 3.1 Hz), 112.9 (d, J = 24.1 Hz), 110.4 (d, J = 8.7 Hz), 106.3 (d, J = 25.7 Hz), 38.6, 31.6, 25.2, 13.7, 10.4. <sup>19</sup>F-{<sup>1</sup>H} NMR (470 MHz, DMSO): δ -122.55 (s, 1F). IR (ATR): 2925, 1716, 1670, 1598, 1556, 1478, 1324, 1198, 801, 606 cm<sup>-1</sup>. LC-MS: Calculated mass for (M+H)<sup>+</sup>: 386.1511, Found: 386.1 (100%). HRMS: Calculated mass for M: 385.1438. Found (M): 385.1434. Difference: -1.01 ppm (99.57% IMS).

2,5-dioxopyrrolidin-1-yl (Z)-4-(5-((5-fluoro-2-oxoindolin-ylidene)methyl)-2,4-dimethyl-1Hpyrrole-3-carboxamido)butanoate (5). 0.4 g (1. mmol, 1 eq.) of acid derivative and 0.21 g (1.9 mmol, 1.78 eq.) of N-hydroxysuccinimide were added to a round bottom flask. The flask was purged with N<sub>2</sub>, prior to addition of 10 ml of DMF. 0.29 mL of DIC (0.23 g, 1.87 mmol, 1.78 equivalents), was added while the reaction vessel was kept under an ice bath. The reaction was stirred for 45 minutes and then allowed to adjust to room temperature. The solution was stirred at room temperature for 16 hours (TLC, CHCl<sub>3</sub>:MeOH = 9:1). The solution was added dropwise to 100 ml of water. The resulting precipitate was collected via vacuum filtration, washed with 2 x 10 ml of H<sub>2</sub>O and dried using a Schlenk line. The crude solid was triturated with 50 mL of chloroform, collected using vacuum filtration, washed with 2 x 30 mL of Chloroform and dried using a Schlenk line (yield: 0.42 g, 82%). <sup>1</sup>H NMR (500 MHz, DMSO): δ 13.68 (s, 1H, pyrrole-NH), 10.89 (s, 1H, indole-NH), 7.78 – 7.67 (m, 3H, ArH/Alkene/amide-NH), 6.92 (td, J = 9.5, 2.4 Hz, 1H, ArH), 6.84 (dd, J = 8.4, 4.5 Hz, 1H, ArH), 3.32 - 3.28 (m, 2H,  $CH_2$ ), 2.82 (s, 4H, NHS- $CH_2$ ), 2.75 (dd, J = 15.2, 7.7 Hz, 2H,  $CH_2$ ), 2.43 (s, 3H,  $CH_3$ ), 2.41 (s, 3H, CH<sub>3</sub>), 1.92 - 1.84 (m, 2H, CH<sub>2</sub>). <sup>13</sup>C NMR (126 MHz, DMSO-d<sup>6</sup>):  $\delta$  170.7, 170.0, 169.3, 165.3, 158.7 (d, J = 234.2 Hz), 136.9, 134.98, 130.7, 127.6, 126.2 (d, J = 9.5 Hz), 125.3, 121.3, 115.0 (d, J = 3 Hz), 112.9 (d, J = 24.2 Hz), 110.5 (d, J = 8.7 Hz), 106.5 (d, J = 25.7 Hz), 38.3, 28.4, 25.9, 25.0, 13.7, 10.9.  $^{19}F-\{^{1}H\}$  NMR (470 MHz, DMSO):  $\delta$  -122.54 (s, 1F). IR (ATR): 2922, 1810, 1781, 1738, 1674, 1567, 1477, 1262, 1197, 1072, 804, 726, 649, 583, 448 cm<sup>-1</sup>. LC-MS: Calculated mass for (M+H)<sup>+</sup>: 483.2, Found: 483.2 (100%). HRMS: Calculated mass for M: 482.1602. Found (M): 482.1602. Difference: 0.14 ppm (99.37% IMS).

 $[Pt(OH)(CI)_2(NH_3)_2((Z)-4-(5-((5-fluoro-2-oxoindolin-3-ylidene)methyl)-2,4-dimethyl-1H$ pyrrole-3-carboxamido)butanoic acid)] (A) 0.28 g of oxoplatin (0.85 mmol, 1.05 equivalents) was added to a round bottom flask. 0.39 g (0.81 mmol, 1 eq.) of NHS-ester was dissolved in 15 ml of DMSO and added. The solution was stirred at 55°C for 16 hours in the absence of light. The reaction mixture was filtered through cotton wool to remove excess oxoplatin. The filtrate was added to 200 ml of deionised water. The precipitate was collected via vacuum filtration and dried using a Schlenk line. The solid was dissolved in 3 mL of DMF. 27 mL of diethyl ether was added and the precipitate was collected via centrifugation. This was repeated 3 times and the solid was subsequently washed with 2 x 20 mL of diethyl ether and dried using a Schlenk line (yield: 0.42 g, 73%). <sup>1</sup>H NMR (500 MHz, DMSO): δ 13.67 (s, 1H, pyrrole-NH), 10.88 (s, 1H, indole-NH), 7.76 (dd, J = 9.4, 2.3 Hz, 1H, ArH), 7.71 (s, 1H, alkene-H), 7.67 - 7.60 (m, 1H, amide-NH), 6.96 - 6.88 (m, 1H. ArH), 6.84 (dd, J = 8.4, 4.6 Hz, 1H, ArH), 6.20 - 5.74 (m, 6H,  $2 \times NH_3$ ), 3.23 (dt, J = 12.9, 6.7 Hz, 2H,  $CH_2$ ), 2.40 (t, J = 13.0 Hz, 3H,  $CH_3$ ), 2.24 (t, J = 7.4 Hz, 3H, CH<sub>3</sub>), 1.72 (dt, J = 14.5, 7.4 Hz, 2H, CH<sub>2</sub>).  $^{13}$ C NMR (126 MHz, DMSO-d<sup>6</sup>):  $\delta$  181.0, 170.0, 165.2, 162.7, 157.7 (d, J = 234.2 Hz), 136.8, 134.9, 130.7, 127.6 (d, J = 49.0 Hz), 126.2, 125.3, 121.5, 114.9 (d, J = 3.0 Hz), 112.9 (d, J = 24.5 Hz), 112.7, 110.5 (d, J = 8.3 Hz), 106.3 (d, J = 25.1 Hz), 38.8, 34.3, 26.3, 13.8, 11.0. <sup>19</sup>F-{<sup>1</sup>H} NMR (470 MHz, DMSO):  $\delta$  -122.55 (s, 1F). <sup>195</sup>Pt NMR (108 MHz, DMSO): δ 1047.36 (s, 1Pt). LC-MS: (100%). IR (ATR): 3196, 1617, 1544, 1475, 1323, 1260, 1197, 1144, 1026, 923, 851, 796, 696, 666, 607, 584, 444 cm<sup>-1</sup>. HRMS: Calculated mass for M: 700.0943. Found: 699.0870 (M-H)-. Difference: -1.4 ppm.

[Pt(OH)(Oxalate)<sub>2</sub>(DACH)<sub>2</sub>((Z)-4-(5-((5-fluoro-2-oxoindolin-3-ylidene)methyl)-2,4-dimethyl-1H-pyrrole-3-carboxamido)butanoic acid)] (B). 0.15 g of dihydroxyoxaliplatin (0.35 mmol, 1.05 equivalents) was added to a round bottom flask. 0.16 g (0.34 mmol, 1 eq.) of NHS-ester was dissolved in 8 ml of DMSO and added. The solution was stirred at 55°C for 16 hours in the absence of light. The reaction mixture was filtered through cotton wool to remove excess oxoplatin. The DMSO solution was added dropwise to 50 mL of water. The resulting precipitate was collected via centrifugation, washed with 2 x 20 mL of water and then dried using a Schlenk line. The solid was dissolved in 3 mL of DMF. 27 mL of diethyl ether was added and the precipitate was collected via centrifugation. This was repeated 3 times and the solid was subsequently washed with 2 x 20 mL of diethyl ether and dried using a Schlenk line (Yield: 0.26 g, 97%). <sup>1</sup>H NMR (500 MHz, DMSO):  $\delta$  13.68 (s, 1H, pyrrole-NH), 10.91 (s, 1H, indole-NH), 8.45 (s, 1H, NH), 8.16 (s, 1H, NH), 7.87 (s, 1H, NH), 7.80 – 7.74 (m, 1H, ArH), 7.71 (s, 1H, NH), 7.68 (t, J = 5.5 Hz, 1H, Amide-NH), 7.15 (s, 1H, alkene-H), 6.96 – 6.89 (m, 1H, ArH), 6.84 (dd, J= 8.3, 4.5 Hz, 1H, ArH), 3.21 (d, J = 6.1 Hz, 2H, CH<sub>2</sub>), 2.56, (s, 2H, CH<sub>2</sub>), 2.42 (s, 3H, CH<sub>3</sub>), 2.40 (s, 3H, CH<sub>3</sub>), 2.27 (t, J = 7.1 Hz, 2H, CH<sub>2</sub>), 2.12 – 2.02 (m, 2H, CH<sub>2</sub>), 1.72 – 1.65 (m, 2H, CH<sub>2</sub>), 1.53 – 1.30 (m, 4H, 2 x CH<sub>2</sub>), 1.12 (d, J = 9.9 Hz, 2H, CH<sub>2</sub>). <sup>13</sup>C NMR (126 MHz, DMSO): δ 182.1, 170.0, 165.2, 164.3 (d, J = 234.4 Hz), 157.7, 136.8, 134.9, 130.7, 127.6 (d, J = 9.6 Hz), 126.2, 125.4, 121.4, 114.9 (d, J = 2.9 Hz), 112.9 (d, J = 23.7 Hz), 110.5 (d, J = 9.2 Hz), 106.5 (d, J = 25.1Hz), 61.8, 60.5, 38.6, 34.5, 26.3, 24.1, 13.7, 11.0.  $^{19}$ F- $^{1}$ H} NMR (471 MHz, DMSO): δ -122.50 (1F, s).  $^{195}$ Pt NMR (108 MHz, DMSO):  $\delta$  1408.01 (s, 1Pt). IR (ATR): 2938, 1723, 1659, 1626, 1567, 1476, 1439, 1320, 1257, 1192, 1160, 1144, 1064, 1026, 921, 848, 804, 777, 663, 584,

444 cm<sup>-1</sup>. HRMS: Calculated mass for M: 797.1928. Found (M): 797.1916. Difference: -1.3 ppm.

[Pt(OH)(CBDCA)<sub>2</sub>(DACH)<sub>2</sub>((Z)-4-(5-((5-fluoro-2-oxoindolin-3-ylidene)methyl)-2,4-dimethyl-1H-pyrrole-3-carboxamido)butanoic acid)] (C). 0.083 g of dihydroxycarboplatin (0.20 mmol, 1.05 equivalents) was added to a round bottom flask. 0.09 g (0.19 mmol, 1 eq.) of NHS-ester was dissolved in 6 ml of DMSO and added. The solution was stirred at 55°C for 16 hours in the absence of light. The DMSO solution was added dropwise to 25 mL of water. The resulting precipitate was collected via centrifugation, washed with 20 mL of water and dried using a Schlenk line. The crude solid was dissolved in 1.5 mL of DMF. 17 mL of diethyl ether was added to the filtrate and the precipitate was collected via centrifugation. This was repeated 3 times and the solid was subsequently washed with 2 x 20 mL of diethyl ether and dried using a Schlenk line (yield: 0.13 g, 80%). <sup>1</sup>H NMR (500 MHz, DMSO): δ 13.68 (s, 1H, pyrrole-NH), 10.91 (s, 1H, indole-NH), 7.77 (dd, J = 9.3, 2.2 Hz, 1H, ArH), 7.72 (s, 1H, alkene-H), 7.67 (t, J = 5.2 Hz, 1H, amide-NH), 6.97 - 6.89 (m, 1H, ArH), 6.85 (dd, J = 8.4, 4.5 Hz, 1H, ArH), 6.12 - 5.74 (m, 6H, 2 x NH<sub>3</sub>), 3.25 - 3.19 (m, 2H, CH<sub>2</sub>), 2.55 (dd, J = 16.0, 10.2 Hz, 2H, CH<sub>2</sub>), 2.47 (d, J = 8.1 Hz, 2H,  $CH_2$ ), 2.42 (s, 3H,  $CH_3$ ), 2.40 (s, 1H,  $CH_3$ ). 2.25 (t, J = 7.5 Hz, 2H,  $CH_2$ ), 1.85 – 1.64 (m, 4H, 2 x CH<sub>2</sub>). <sup>13</sup>C NMR (126 MHz, DMSO): δ 180.4, 177.0, 170.0, 165.1, 158.7 (d, J = 234. 1 Hz), 136.8, 134.9, 130.7, 127.6 (d, J = 9.6 Hz), 126.2, 125.4, 121.5, 114.9 (d, J = 2.8 Hz), 110.4 (d, J = 8.1Hz), 106.5 (d, J = 25.2 Hz), 56.1, 38.8, 32.8, 31.7, 26.3, 16.3, 13.7, 10.9. <sup>19</sup>F-{<sup>1</sup>H} NMR (471 MHz, DMSO):  $\delta$  -122.54 (1F, s). <sup>195</sup>Pt NMR (108 MHz, DMSO):  $\delta$  1756.48 (s, 1Pt). IR (ATR): 3221, 1626, 1568, 1476, 1438, 1321, 1257, 1194, 1160, 1145, 1095, 1026, 919, 849, 796, 664, 585, 469, 445 cm<sup>-1</sup>. HR-MS: Calculated mass for M: 772.1832. Found: (M+H)<sup>+</sup>. Difference: -7.5 ppm.

# **Results & Discussion**

#### **Syntheses**

As highlighted in our group's recent review on metal-TKI conjugates<sup>46</sup>, a crucial aspect TKI functionalization is preserving kinase inhibitory activity that requires modifications in the solvent-exposed regions. Docking studies of sunitinib with VEGFR2 by Wang et al. <sup>47</sup> and Peng et al. <sup>48</sup> revealed that the diethylaminoethyl functional group of Sunitinib does not engage the active site of the protein. Functionalization at this position is therefore unlikely to compromise active site binding and experimental evidence further indicates that functionalisation within this hydrophilic moiety is well tolerated<sup>47</sup>. Sunitinib derivatives maintained excellent activity against PDGFRα, VEGFR and c-KIT, when compared to sunitinib itself<sup>49</sup>. For example, Argyros et al. synthesized a sunitinib-peptide conjugate that retained excellent kinase inhibitory activity despite its sterically demanding macrocyclic peptide moiety<sup>49</sup>. Guided by this rationale, we designed and synthesised three Pt(IV)-sunitinib conjugates A, B and C (Figure 2) with functionalisation exclusively at the diethylaminoethyl moiety (Scheme 1).

**Scheme 1.** Synthesis of the three Pt(IV) – Sunitinib prodrugs: (i) 5-fluorooxindole, piperidine, EtOH, 80°C, 3 h, 84% (ii) γ-aminobutyric methyl ester, TBTU, TEA, DMF r.t., 24 h, 41% (iii) 1M NaOH, MeOH/H<sub>2</sub>O, r.t., 24 h, 86% (iv) DIC, DMF, r.t., 24 h, 82% (v) oxoplatin, DMSO, 55°C, 16 h, 73% (vi) dihydroxyoxaliplatin, DMSO, 55°C, 16 h, 97% (vii) dihydroxycarboplatin, DMSO, 55°C, 16 h, 80%.

C = R is carboplatin scaffold

Overall, an NHS-ester strategy was implemented to synthesize all three Pt(IV) complexes. NHS-activation has previously been shown by our group to be a highly successful strategy to synthesize Pt(IV) prodrugs<sup>35,50–52</sup>. The initial reaction involves a Knovenegal condensation between 5-fluorooxindole and 5-formyl-dimethyl-1H-pyrrole-3-carboxylic acid (1) to yield carboxylic acid conjugate, 2, in excellent yield. Here, it was decided to conjugate this carboxylic acid derivative to a Pt(IV) scaffold, again using the NHS-conjugation strategy. However, the reaction of the NHS-ester derivative of 2 with oxoplatin did not indicate the formation of a mono-axial functionalised Pt(IV) derivative as desired. Hence, we incorporated a C3 linker into the sunitinib moiety as this has been shown to alleviate the possible steric problems previously encountered in the synthesis of Pt(IV)-imatinib complexes<sup>35</sup>. The C3 linker would provide sufficient distance between the sunitinib moiety and the Pt(IV) scaffold, maintaining interactions in the binding sites of VEGFR, PDGFR and c-KIT. As such, amide coupling of 2 with y-aminobutyric methyl ester using TBTU as the coupling agent yields the formation of the methyl ester, 3. Base deprotection of the methyl ester provided the desired carboxylic acid derivative, 4, in excellent yield. Finally, after optimisation of the reaction conditions, the NHS-ester, 5, was synthesized by using N,N'-diisopropylcarbodiimide as coupling agent. Conjugation of 5 with cisplatin-, oxaliplatin-, and carboplatin-derived Pt(IV) precursors proceeded efficiently (73-97% yield) with minimal optimization, yielding complexes A, B, and C. The final complexes were characterised by 1D and 2D multinuclear NMR (<sup>1</sup>H, <sup>13</sup>C, <sup>19</sup>F, <sup>195</sup>Pt) spectroscopy, IR spectroscopy and high-resolution mass spectrometry and the purity and the stability of the complexes was assessed using LC-MS (Figures S1-S7).

#### **Stability Studies**

The stability of the complexes was assessed over a 72-hour period using LC-MS in 1:1 (v/v) DMSO: RPMI 1640 cell culture medium solution, at 37 °C, (**Figure S8-10**). Complexes **B** and **C** were sufficiently stable in the DMSO:RPMI mixture within 72 hours, retaining >87% of intact Pt(IV) species after 72 hours while complex **A** underwent significant decomposition under these conditions. After 72 hours, only 41.3% of the complex remained intact (r.t. = 28 min, **Figure S8**), while 14.1% was identified as free carboxylic acid ligand **4** (r.t. = 30 min, m/z (M+H) $^+$  = 386.1)), indicating the release of the axial ligand. More intriguingly, an unexpected

third peak accounted for 44.7% of the composition was found at an earlier retention time (r.t. = 26 min). Analysis of the corresponding mass-spectrum (Figure S8) and the fragmentation pattern identified the dominant decomposition product (m/z 680) as a mono-hydroxo-aquated Pt(IV) species [Pt(4)(OH<sub>2</sub>)(NH<sub>3</sub>)<sub>2</sub>Cl(OH)]<sup>+</sup> (with literature precedent<sup>61</sup>). This mono-aquation is rather unexpected for cisplatin-derived Pt(IV) prodrugs, which are typically kinetically inert. Notably, <sup>62</sup> the observed decomposition of complex A contrasts sharply with the observed stability of complexes B and C under identical conditions<sup>62</sup>. The hydrolytic product of A is expected to behave similar fashion as A itself, as after reduction, the two intracellularly released moieties would be the axial sunitinib ligand and the mono-aquated, active form of cisplatin. As such, the stability was deemed sufficient to continue assessments of each complex. The reduction of the three complexes in DMSO:PBS 1:1 by an excess of ascorbic acid (10 equivalents) was followed by LCMS (Figure 4 and S11-13) and NMR (Figure S14). Both complex A and complex C were fully reduced within 24 hours, while complex B had a negligible amount of intact complex remaining even after 72 hours (~14.5%).

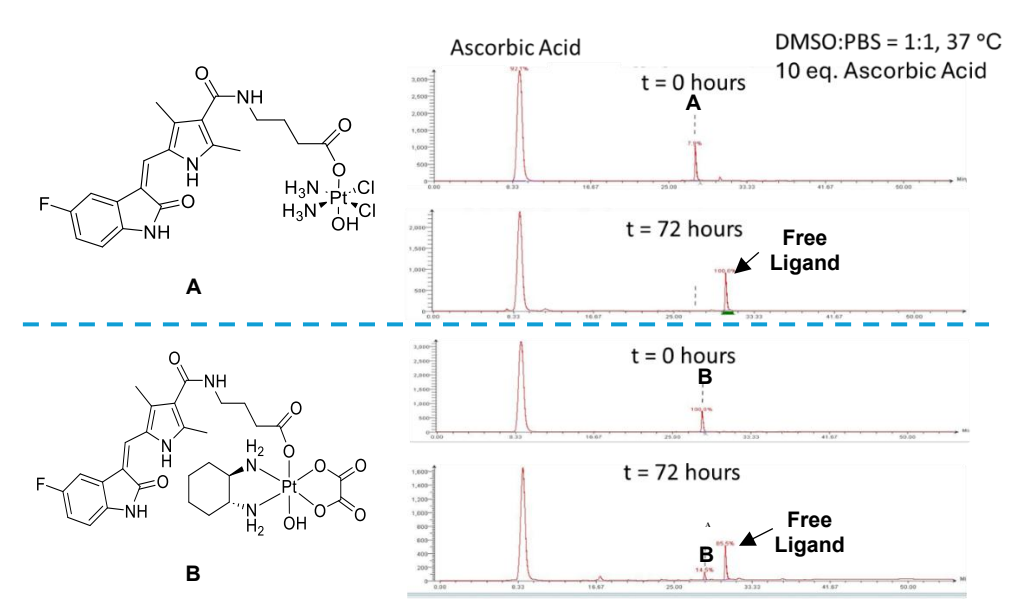


**Figure 4.** Reduction of complex **A** (top) and complex **B** (bottom) as followed by LCMS. The peak at 31 min is the released axial free ligand, confirming reduction of the Pt(IV) complexes. Reduction of **C** can be found in the ESI (**Figure S13**).

#### **Electrochemical Studies**

The redox behaviour of both the released upon reduction carboxylic acid ligand **4**, and each Pt(IV) complex was further characterized by cyclic voltammetry (CV), **Figure 5** and **Figure S15-19**. Compound **4** displayed only one reduction peak at  $E_p^c = -1.82$  V vs Ag/Ag<sup>+</sup> (Peak I, **Figure 5**), consistent with the literature values for sunitinib ( $E_p^c = -1.90$  V vs Ag/Ag<sup>+</sup>, when a slightly different solvent system was implemented i.e. 10% DMSO in ACN<sup>63</sup>). This one-electron process is attributed to reduction of the indole ring<sup>63</sup>.

CVs of each complex were compared with ligand 4 to determine their Pt(IV)/Pt(II) reduction potentials. Figure 5 illustrates this for complex A, showing the ligand's reduction peak ( $E_p^c = -1.82 \text{ V vs. Ag/Ag}^+$ ) alongside a second peak at  $E_p^c = -1.36 \text{ V (Peak II)}$  corresponding to Pt(IV)/Pt(II) reduction. This value aligns with literature reports for monoaxial cisplatin-based Pt(IV) prodrugs<sup>64</sup>. Applying the same method as above for B and C (Figures S15-S19), the Pt(IV/II) reduction potentials were determined to be as follows: -1.36 V for A, -1.54 V for B, and -1.58 V for C. Notably, the observed reduction rates ( $A \ge C > B$ ) invert the thermodynamic trend implied by reduction potentials (A >> B > C). This kinetic vs. thermodynamic disparity is consistent with established Pt(IV) prodrug behaviour.

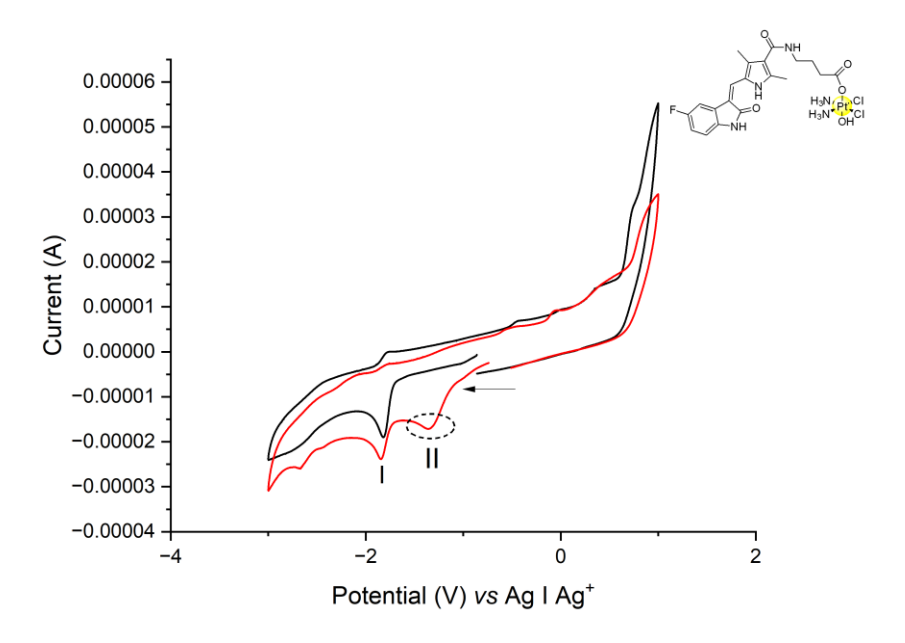


**Figure 5.** The cyclic voltammogram of complex **A** overlayed with **4**. The experiment was performed at the same concentration ([compound] = 2 mM) in 0.1 M DMSO-[n-Bu<sub>4</sub>N][PF<sub>6</sub>] at a scan rate of 0.1 Vs<sup>-1</sup>. Legend: **4** = Red, complex **A** = Black .

#### **Biological Studies**

#### **Enzyme Inhibition Assays**

The inhibitory activity of Pt(IV) complexes **A-C** and of the free ligand **4** against isolated VEGFR2, PDGFR $\beta$  and c-KIT kinases was evaluated, with IC<sub>50</sub> values summarized in **Figure 6**. 65 All compounds retained nanomolar activity against all three kinases. Against VEGFR2, complexes **A-C** showed only a marginal decrease in activity compared to sunitinib (IC<sub>50</sub> = ~ 100 vs 79.5 nM). For PDGFR $\beta$  and c-KIT, the activity reduction was more pronounced (e.g. IC<sub>50</sub> for **C** and Sunitinib vs PDGFR $\beta$  = 71.7 and 2.4 nM, respectively). Importantly, the axial ligand **4** (released intracellularly upon Pt(IV) reduction) maintained strong kinase inhibition, confirming that functionalization preserved TKI activity, thereby validating the design strategy of modifying solvent-exposed regions.

	PDGFR-β	VEGFR-2	c-KIT	
	(nM)	(nM)	(nM)	
4	11.5 ± 2.2	83.2 ± 4.1	89.4 ± 5.5	
Α	59.3 ± 4.6	101.9 ± 8.8	162 ± 18.8	
В	69.4 ± 5.9	99.3 ± 6.9	185 ± 25.1	
C	71.7 ± 5.5	105.8 ± 11.5	175 ± 22.3	
Sunitinib	2.4 ± 0.6	79.5 ± 2.4	81.4 ± 6	

	PDGFRβ	VEGFR2	cKIT
4			
Α			
В			
С			
Sunitinib			



**Figure 6.** Inhibition of isolated enzyme isoforms of VEGFR2, PDGR- $\beta$  and c-KIT. Top: IC<sub>50</sub> values (nM) for inhibition of tested compounds **A, B, C** and **4** (at 0.2 μM). Bottom: Heat-map displaying showing the relative inhibition of tested compounds **A, B, C** and **4** (at 0.2 μM). Data are the means of three independent experiments.

## 2D cytotoxicity studies

The cytotoxicity of the Pt(IV) complexes **A**, **B** and **C** together with the free carboxylic acid derivative **4**, was tested by MTT assay (**Table 1**). The complexes were tested against three different cell lines: human renal cell carcinoma (786-O), murine renal cell carcinoma (Renca) and non-cancerous lung fibroblast cell lines (MRC-5) with 72 h incubation time. The 786-O RCC cell line was selected as a clinically relevant model, reflecting sunitinib's FDA-approved use against RCC<sup>36</sup>. This cell line is known to express high levels of VEGFR<sup>70</sup> and PDGFR.<sup>71,72</sup>

**Table 1.** IC<sub>50</sub> Cytotoxicity values ( $\mu$ M) of **A, B, C, 4** and cisplatin determined by MTT assay after 72 hours of exposure.

Compound	786-O <sup>a</sup>	Renca <sup>a</sup>	MRC-5 <sup>a</sup>
4	>130 <sup>b</sup>	>130	>130
Α	$0.50 \pm 0.10$	$0.10 \pm 0.02$	$0.43 \pm 0.11$
В	>20	>20	$6.3 \pm 1.8$
C	>46	>46	13 ± 2
Cisplatin	18 ± 4	$1.1 \pm 0.2$	$2.3 \pm 0.8$

<sup>&</sup>lt;sup>a</sup>Effective concentrations of 50% in 786-O (human renal cell carcinoma), Renca (murine renal cell carcinoma) and MRC-5 (human lung fibroblasts) determined by means of the MTT assay with the exposure time of 72 h. Values are means ± standard deviations obtained fromat least three independent experiments. <sup>b</sup> The maximum tested concentrations were limited by the solubility of the compounds in DMSO.

The MTT assay results demonstrated notable variations in the cytotoxic effects of sunitinib-derived ligand 4 and its Pt(IV) conjugates A-C (Table 1). The ligand 4 did not show any cytotoxicity, with IC50 values exceeding 130  $\mu$ M in all tested cell lines, potentially because of reduced cellular uptake when sunitinib is functionalised with a carboxylic acid. In contrast, the Pt(IV)-sunitinib-cisplatin conjugate A exhibited remarkable cytotoxicity in a low micromolar range, demonstrating exceptional potency across all tested cancer cell lines. Complex A showed comparable cytotoxicity against both MRC-5 and 786-O cells, revealing no

preferential activity against renal cancer cells. Most importantly, **A** was orders of magnitude more potent than either of its individual components (**4** or cisplatin) in all cancer models, strongly supporting a synergistic (or at least additive) mechanism resulting from the conjugation. The remaining conjugates, Pt(IV)-sunitinib-oxaliplatin **B** and Pt(IV)-sunitinib-carboplatin **C**, demonstrated minimal cytotoxicity across all the cancer cell lines (IC50 >20  $\mu$ M and >46  $\mu$ M, respectively). Surprisingly, however, they exhibited moderate activity against normal MRC-5 fibroblasts (**B**: 6.3  $\pm$  1.8  $\mu$ M; **C**: 13  $\pm$  2  $\mu$ M). This striking contrast underscores that the platinum drug moiety is a critical determinant of anti-cancer efficacy, with the cisplatin-based conjugate **A** proving dramatically more effective than its oxaliplatin or carboplatin counterparts. Cisplatin alone showed moderate cytotoxicity against 786-O (18  $\pm$  4  $\mu$ M), with notably higher potency against Renca (1.1  $\pm$  0.2  $\mu$ M). It also displayed activity in MRC-5 cells (2.3  $\pm$  0.8  $\mu$ M). These results highlight the exceptional enhancement achieved by conjugation of cisplatin and sunitib-derived ligand in **A**. However, the lack of *in-vitro* activity shown by complex **B** and **C** was of both interest and concern. We hypothesized that the lower cellular uptake of **B** and **C** compared to **A** may play a role in their reduced activity.

### Cellular Uptake

In order to assess potential correlations between cytotoxic activity and intracellular accumulation, we performed cellular uptake experiments in 786-O cells. The cells were treated with A-C or cisplatin at equimolar (1  $\mu$ M) concentrations, and Pt accumulation was evaluated by GF-AAS at 12 h and 24 h time points (Figure 7).

The results revealed striking differences in intracellular accumulation of Pt(IV) complexes. Complex A demonstrated superior and time-dependent accumulation in cancer cells, achieving intracellular Pt levels up to 18-fold higher than cisplatin. In contrast, complexes B and C showed substantially lower uptake, mirroring cisplatin's poor cell uptake These studies provide a mechanistic explanation for the previously observed differences in cytotoxic activity between complexes A-C. The exceptional cellular internalization of complex A directly correlated with its enhanced cytotoxic potency, while the limited uptake of complexes B, C and cisplatin aligns with their reduced activity.

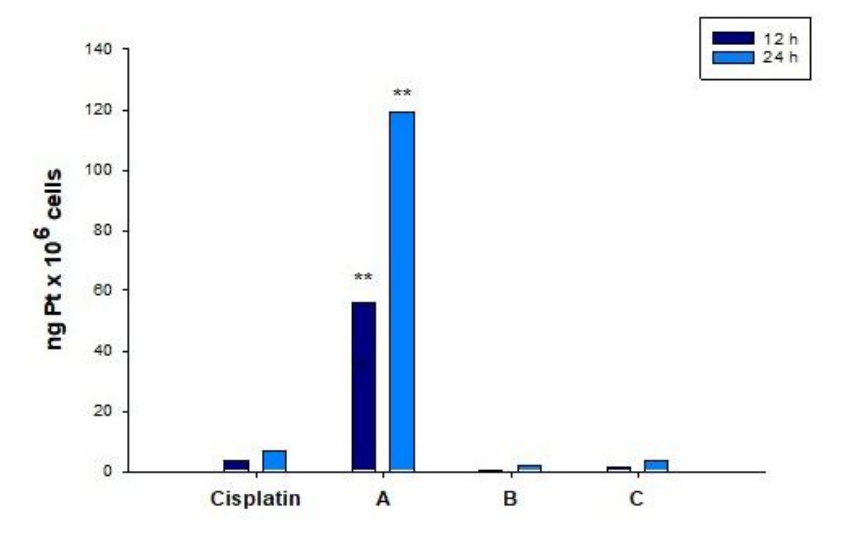


**Figure 7.** Cellular uptake. 786-O cancer cells were incubated with equitoxic concentrations (1  $\mu$ M) of **A, B, C** and cisplatin for 12 or 24 h, and cellular platinum content was detected by GF-AAS analysis. Error bars indicate the standard deviation. \*\*p<0.05

### 3D cytotoxicity

While conventional 2D cell cultures remain widely employed for *in vitro* drug screening due to their cost-effectiveness and reliability, they fail to properly reproduce the complex microenvironment of solid tumors. In contrast, 3D cell culture models better mimic tumor heterogeneity and have demonstrated superior predictive value for *in vivo* outcomes<sup>73</sup>. To evaluate compound performance in a more physiologically relevant model, we tested the complexes **A-C** in renal cancer cell spheroids for 72 h by means of the acid phosphatase (APH) assay (**Table 2**). Consistent with the 2D results, complex **A** emerged as the most active compound, exhibiting 7-fold higher activity than cisplatin. Complexes **B** and **C** again showed no activity, likely due to their poor cellular uptake as observed in previous permeation studies.

**Table 2.** 3D cytotoxicity against renal cancer cell spheroids.

IC <sub>50</sub> (μM) ± S.D. 786-O <sup>a</sup>				
Α	6.4 ± 3.9			
В	>200			
С	>200			
Cisplatin	45.1 ± 5.3			

<sup>&</sup>lt;sup>a</sup> Spheroids (1.5×10<sup>3</sup> cells/well) were treated for 72 h with increasing concentrations of test compounds. The growth inhibitory effect was evaluated by means of the APH test.  $IC_{50}$  values were calculated from the dose-survival curves by the four parameter logistic model (P < 0.05). SD=standard deviation. Data are the means of three independent experiments.

#### *In-vivo orthotopic RCC model*

The orthotopic RCC mouse model study provided compelling validation of the *in vivo* potential of complex **A** in comparison with cisplatin (**Figure 8**). Tumour progression and treatment efficacy were systematically evaluated through longitudinal measurements of tumour volume (calculated as [length × width²]/2) and body weight (assessing systemic toxicity), with treatments administered on Days 40, 42, and 44, and terminal analysis on Day 45. **A** exhibited exceptional tumour suppression, achieving an 81% reduction in mean tumour volume versus vehicle control (152 mm³ vs. 806 mm³) and a 68% improvement over cisplatin (483 mm³). While vehicle-treated tumours displayed aggressive, heterogeneous growth (332–1527 mm³) and cisplatin showed variable efficacy (84–803 mm³), **A** demonstrated remarkable consistency across all mice (56–226 mm³), including one mouse with near-complete regression (56 mm³).

Critically, complex  $\bf A$  also displayed enhanced safety in comparison with cisplatin, underscoring its therapeutic potential. Mice treated with  $\bf A$  and vehicle experienced only mild weight loss ( $\sim$ 1.33 g and  $\sim$ 1.53 g, respectively), attributable to tumour burden rather than toxicity of the treatment. In contrast, cisplatin induced higher weight loss ( $\sim$ 2.23 g), consistent with its known adverse effects in patients. These findings position complex  $\bf A$  as a promising candidate for RCC therapy, combining robust antitumor activity with a favourable tolerability.

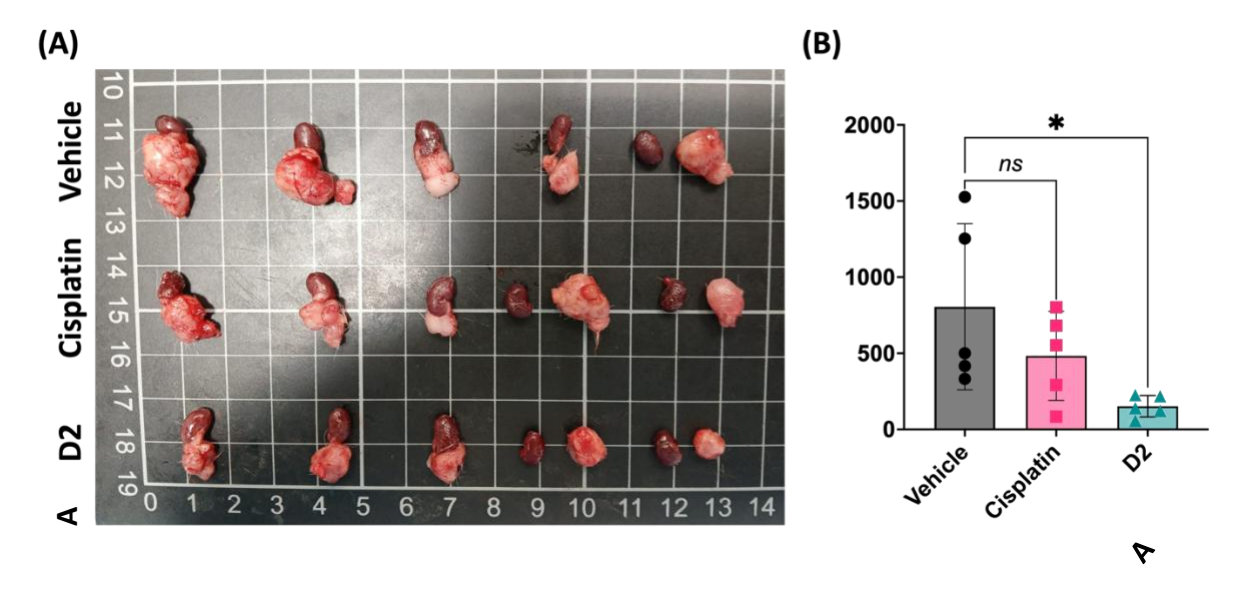


**Figure 8. (A)** Representative tumour pictures: high-resolution images of orthotopically implanted renal cell carcinoma tumours within murine kidneys across treatment groups.

**(B)** Tumour volume change at the endpoint: a bar graph depicting the change in tumour volume at the experimental endpoint (Day 45).

## Conclusion

The severe drawbacks of clinically used platinum(II) and tyrosine kinase inhibitor anti-cancer compounds has led to research into combination therapy of both in order to overcome resistance and potentially reduce side effects. To date, only four Pt(IV)-TKI conjugates have been reported in literature: Pt(IV)-Gefitinib, Pt(IV)-Erlotinib, Pt(IV)-Dasatinib, and Pt(IV)-Imatinib/Nilotinib derivatives. In this study, we presented the first series of Pt(IV) complexes targeting VEGFR through rationally designed sunitinib derivatives. The hydrolytic stability of these novel complexes was of considerable importance, as the hydrolysis of the equatorial ligands differed greatly to what is observed in the literature<sup>62</sup>. Comprehensive characterization through CV and LCMS reduction studies proved the potential of these complexes to act as effective prodrugs. Importantly, enzyme inhibition assays demonstrated that the functionalisation of sunitinib, had not jeopardized its kinase inhibitory activity.

Among the synthesized compounds, the cisplatin-based Pt(IV)-sunitinib prodrug **A** emerged as the clear lead candidate, exhibiting substantially greater anticancer activity compared to oxaliplatin and carboplatin counterparts across the renal cancer cell lines. The superior performance of complex **A** was directly correlated with its enhanced cellular uptake. The promising results from adherent 2D cell culture experiments were further validated in 3D spheroid models, warranting its progression into *in vivo* studies. In orthotopic RCC (Renal Cell Carcinoma) allograft models using BALB/c mice, complex **A** demonstrated significantly improved efficacy compared to cisplatin, while maintaining a much more favourable toxicity profile. These compelling results highlight its potential as a next-generation anticancer agent against RCC. Future studies will focus on enhancing the aqueous solubility of these conjugates and optimising new synthetic protocols to enable precise modulation of their targeting/uptake characteristics and reductive properties through strategic functionalisation of the second axial position. In addition, we plan to explore the therapeutic potential of these

complexes against other tumour types, such as colorectal cancer, to broaden their clinical applicability.

#### **Conflicts of Interest**

There are no conflicts to declare.

## **Acknowledgements**

The author D.F.B. would like to thank the Irish Research Council for funding the research via a Government of Ireland Postgraduate Scholarship (GOIPG/2020/55). M.V.B. acknowledges support from Collaborative Research Fund (CRF) (8730107). D.M and T.V.T thankfully acknowledge support from Science Foundation Ireland (SFI): SFI 2012 Strategic Opportunity Fund (Infrastructure award 12/RI/2346/SOF) for NMR facilities and SFI Opportunistic Infrastructure Fund 2016 (16/RI/3399) for LC-MS.

#### References

- (1) Einhorn, L. H. Treatment of Testicular Cancer: A New and Improved Model. *Journal of Clinical Oncology* **1990**, *8* (11), 1777–1781. https://doi.org/10.1200/JCO.1990.8.11.1777.
- (2) Tesniere, A.; Schlemmer, F.; Boige, V.; Kepp, O.; Martins, I.; Ghiringhelli, F.; Aymeric, L.; Michaud, M.; Apetoh, L.; Barault, L.; Mendiboure, J.; Pignon, J. P.; Jooste, V.; Van Endert, P.; Ducreux, M.; Zitvogel, L.; Piard, F.; Kroemer, G. Immunogenic Death of Colon Cancer Cells Treated with Oxaliplatin. *Oncogene* 2010, 29 (4), 482–491. https://doi.org/10.1038/onc.2009.356.
- (3) Coleman, R. L.; Broaddus, R. R.; Bodurka, D. C.; Wolf, J. K.; Burke, T. W.; Kavanagh, J. J.; Levenback, C. F.; Gershenson, D. M. Phase II Trial of Imatinib Mesylate in Patients with Recurrent Platinum- and Taxane-Resistant Epithelial Ovarian and Primary Peritoneal Cancers. *Gynecol Oncol* 2006, 101 (1), 126–131. https://doi.org/10.1016/j.ygyno.2005.09.041.
- (4) Lokich, J. What Is the "Best" Platinum: Cisplatin, Carboplatin, or Oxaliplatin? *Cancer Invest* **2001**, *19* (7), 756–760. https://doi.org/10.1081/CNV-100106152.
- (5) Johnstone, T. C.; Park, G. A. Y.; Lippard, S. J. Mechanism of Action of Classical Platinum Agents. *Anticancer Res* **2014**, *476*, 471–476.
- (6) Shahid, F.; Farooqui, Z.; Khan, F. Cisplatin-Induced Gastrointestinal Toxicity: An Update on Possible Mechanisms and on Available Gastroprotective Strategies. *Eur J Pharmacol* **2018**, *827* (December 2017), 49–57. https://doi.org/10.1016/j.ejphar.2018.03.009.
- (7) El-Awady, E. S. E.; Moustafa, Y. M.; Abo-Elmatty, D. M.; Radwan, A. Cisplatin-Induced Cardiotoxicity: Mechanisms and Cardioprotective Strategies. *Eur J Pharmacol* **2011**, 650 (1), 335–341. https://doi.org/10.1016/j.ejphar.2010.09.085.
- (8) Kanat, O.; Ertas, H.; Caner, B. Platinum-Induced Neurotoxicity: A Review of Possible Mechanisms. *World J Clin Oncol* **2017**, *8* (4), 329–333. https://doi.org/10.5306/wjco.v8.i4.329.
- (9) Rademaker-Lakhai, J. M.; Crul, M.; Zuur, L.; Baas, P.; Beijnen, J. H.; Simis, Y. J. W.; Van Zandwijk, N.; Schellens, J. H. M. Relationship between Cisplatin Administration and the Development of Ototoxicity. *Journal of Clinical Oncology* **2006**, *24* (6), 918–924. https://doi.org/10.1200/JCO.2006.10.077.

- (10) Dentino, M.; Luft, F. C.; Yum, M. N.; Williams, S. D.; Einhorn, L. H. Long Term Effect of Cis-Diamminedichloride Platinum (CDDP) on Renal Function and Structure in Man. Cancer 1978, 41 (4), 1274–1281. https://doi.org/10.1002/1097-0142(197804)41:4<1274::AID-CNCR2820410410>3.0.CO;2-F.
- (11) Ries, F.; Klastersky, J. Nephrotoxicity Induced by Cancer Chemotherapy With Special Emphasis on Cisplatin Toxicity. *American Journal of Kidney Diseases* **1986**, *8* (5), 368–379. https://doi.org/10.1016/S0272-6386(86)80112-3.
- (12) Galluzzi, L.; Vitale, I.; Michels, J.; Brenner, C.; Szabadkai, G.; Harel-Bellan, A.; Castedo, M.; Kroemer, G. Systems Biology of Cisplatin Resistance: Past, Present and Future. Cell Death Dis 2014, 5 (5), e1257-18. https://doi.org/10.1038/cddis.2013.428.
- (13) Galluzzi, L.; Senovilla, L.; Vitale, I.; Michels, J.; Martins, I.; Kepp, O.; Castedo, M.; Kroemer, G. Molecular Mechanisms of Cisplatin Resistance. *Oncogene* **2012**, *31* (15), 1869–1883. https://doi.org/10.1038/onc.2011.384.
- (14) Choy, H. Satraplatin: An Orally Available Platinum Analog for the Treatment of Cancer. *Expert Rev Anticancer Ther* **2006**, *6* (7), 973–982. https://doi.org/10.1586/14737140.6.7.973.
- (15) Petruzzella, E.; Sirota, R.; Solazzo, I.; Gandin, V.; Gibson, D. Triple Action Pt(Iv) Derivatives of Cisplatin: A New Class of Potent Anticancer Agents That Overcome Resistance. *Chem Sci* **2018**, *9* (18), 4299–4307. https://doi.org/10.1039/c8sc00428e.
- (16) Reiber, H.; Ruff, M.; Uhr, M. Ascorbate Concentration in Human Cerebrospinal Fluid (CSF) and Serum. Intrathecal Accumulation and CSF Flow Rate. *Clinica Chimica Acta* **1993**, *217* (2), 163–173. https://doi.org/10.1016/0009-8981(93)90162-W.
- (17) Dong, J.; Huo, S.; Shen, S.; Xu, J.; Shi, T.; Elding, L. I. Reactivity of the Glutathione Species towards the Reduction of Ormaplatin (or Tetraplatin). *Bioorg Med Chem Lett* **2016**, *26* (17), 4261–4266. https://doi.org/10.1016/j.bmcl.2016.07.046.
- (18) Dabbish, E.; Ponte, F.; Russo, N.; Sicilia, E. Antitumor Platinium(IV) Prodrugs: A Systematic Computational Exploration of Their Reduction Mechanism by I -Ascorbic Acid. *Inorg Chem* **2019**, No. Iv. https://doi.org/10.1021/acs.inorgchem.8b03486.
- (19) Ponte, F.; Russo, N.; Sicilia, E. Insights from Computations on the Mechanism of Reduction by Ascorbic Acid of PtIV Prodrugs with Asplatin and Its Chlorido and Bromido Analogues as Model Systems. *Chemistry A European Journal* **2018**, *24* (38), 9572–9580. https://doi.org/10.1002/chem.201800488.
- (20) Zheng, Y. R.; Suntharalingam, K.; Johnstone, T. C.; Yoo, H.; Lin, W.; Brooks, J. G.; Lippard, S. J. Pt(IV) Prodrugs Designed to Bind Non-Covalently to Human Serum Albumin for Drug Delivery. *J Am Chem Soc* **2014**, *136* (24), 8790–8798. https://doi.org/10.1021/ja5038269.
- (21) Li, X.; Liu, Y.; Tian, H. Current Developments in Pt(IV) Prodrugs Conjugated with Bioactive Ligands. *Bioinorganic Chemistry and Applications*. Hindawi Limited 2018. https://doi.org/10.1155/2018/8276139.
- (22) Babu, T.; Sarkar, A.; Karmakar, S.; Schmidt, C.; Gibson, D. Multiaction Pt(IV) Carbamate Complexes Can Codeliver Pt(II) Drugs and Amine Containing Bioactive Molecules. *Inorg Chem* **2020**, *59* (7), 5182–5193. https://doi.org/10.1021/acs.inorgchem.0c00445.
- (23) Yempala, T.; Babu, T.; Karmakar, S.; Nemirovski, A.; Ishan, M.; Gandin, V.; Gibson, D. Expanding the Arsenal of Pt IV Anticancer Agents: Multi-action Pt IV Anticancer Agents with Bioactive Ligands Possessing a Hydroxy Functional Group. *Angewandte Chemie* **2019**, *131* (50), 18386–18391. https://doi.org/10.1002/ange.201910014.

- (24) Paul, M. K.; Mukhopadhyay, A. K. Tyrosine Kinase Role and Significance in Cancer. *Int J Med Sci* **2012**, *1* (283), 101–115. https://doi.org/10.7150/ijms.1.101.
- (25) Carvalho, I.; Milanezi, F.; Martins, A.; Reis, R. M.; Schmitt, F. Overexpression of Platelet-Derived Growth Factor Receptor α in Breast Cancer Is Associated with Tumour Progression. *Breast Cancer Research* **2005**, *7* (5). https://doi.org/10.1186/bcr1304.
- (26) Hansel, D. E.; Rahman, A.; Hermans, J.; De Krijger, R. R.; Ashfaq, R.; Yeo, C. J.; Cameron, J. L.; Maitra, A. Liver Metastases Arising from Well-Differentiated Pancreatic Endocrine Neoplasms Demonstrate Increased VEGF-C Expression. *Modern Pathology* **2003**, *16* (7), 652–659. https://doi.org/10.1097/01.MP.0000077416.68489.50.
- (27) Fjällskog, M. L. H.; Lejonklou, M. H.; Öberg, K. E.; Eriksson, B. K.; Janson, E. T. Expression of Molecular Targets for Tyrosine Kinase Receptor Antagonists in Malignant Endocrine Pancreatic Tumors. *Clinical Cancer Research* **2003**, *9* (4), 1469–1473.
- (28) Fjällskog, M. L.; Hessman, O.; Eriksson, B.; Janson, E. T. Upregulated Expression of PDGF Receptor Beta in Endocrine Pancreatic Tumors and Metastases Compared to Normal Endocrine Pancreas. *Acta Oncol (Madr)* **2007**, *46* (6), 741–746. https://doi.org/10.1080/02841860601048388.
- (29) Board, R.; Jayson, G. C. Platelet-Derived Growth Factor Receptor (PDGFR): A Target for Anticancer Therapeutics. *Drug Resistance Updates* **2005**, *8* (1–2), 75–83. https://doi.org/10.1016/j.drup.2005.03.004.
- (30) Manzat Saplacan, R. M.; Balacescu, L.; Gherman, C.; Chira, R. I.; Craiu, A.; Mircea, P. A.; Lisencu, C.; Balacescu, O. The Role of PDGFs and PDGFRs in Colorectal Cancer. *Mediators Inflamm* 2017, 2017. https://doi.org/10.1155/2017/4708076.
- (31) Betsholtz, C. Biology of Platelet-Derived Growth Factors in Development. *Birth Defects Res C Embryo Today* **2003**, *69* (4), 272–285. https://doi.org/10.1002/bdrc.10030.
- (32) Caban, M.; Fronik, P.; Terenzi, A.; Federa, A.; Bormio Nunes, J. H.; Pitek, R.; Kirchhofer, D.; Schueffl, H. H.; Berger, W.; Keppler, B. K.; Kowol, C. R.; Heffeter, P. A New Fluorescent Oxaliplatin(Iv) Complex with EGFR-Inhibiting Properties for the Treatment of Drug-Resistant Cancer Cells. *Inorg Chem Front* **2025**. https://doi.org/10.1039/d4qi03025g.
- (33) Li, R.; Zhao, W.; Jin, C.; Xiong, H. Novel 4-Amino-Quinazoline Moieties Ligated Platinum(IV) Prodrugs Overcome Cisplatin Resistance in EGFRWT Human Lung Cancer. *Bioorg Chem* **2023**, *135* (April), 106499. https://doi.org/10.1016/j.bioorg.2023.106499.
- (34) Markova, L.; Maji, M.; Kostrhunova, H.; Novohradsky, V.; Kasparkova, J.; Gibson, D.; Brabec, V. Multiaction Pt(IV) Prodrugs Releasing Cisplatin and Dasatinib Are Potent Anticancer and Anti-Invasive Agents Displaying Synergism between the Two Drugs. *J Med Chem* **2024**, No. Iv. https://doi.org/10.1021/acs.jmedchem.4c00888.
- (35) Beirne, D. F.; Farkaš, B.; Donati, C.; Gandin, V.; Rozas, I.; Velasco-Torrijos, T.; Montagner, D. Novel Design of Dual-Action Pt(Iv) Anticancer pro-Drugs Based on Cisplatin and Derivatives of the Tyrosine Kinase Inhibitors Imatinib and Nilotinib. *Dalton Transactions* **2023**, *52* (39), 14110–14122. https://doi.org/10.1039/d3dt02030d.

- (36) FDA. FDA Approves New Treatment for Gastrointestinal and Kidney Cancer. https://web.archive.org/web/20060203031129/http://www.fda.gov/bbs/topics/new s/2006/NEW01302.html.
- (37) Sonpavde, G.; Jian, W.; Liu, H.; Wu, M. F.; Shen, S. S.; Lerner, S. P. Sunitinib Malate Is Active against Human Urothelial Carcinoma and Enhances the Activity of Cisplatin in a Preclinical Model. *Urologic Oncology: Seminars and Original Investigations* **2009**, *27* (4), 391–399. https://doi.org/10.1016/j.urolonc.2008.03.017.
- (38) Yoon, Y. K.; Im, S. A.; Min, A.; Kim, H. P.; Hur, H. S.; Lee, K. H.; Han, S. W.; Song, S. H.; Youn Oh, D.; Kim, T. Y.; Ho Kim, W.; Bang, Y. J. Sunitinib Synergizes the Antitumor Effect of Cisplatin via Modulation of ERCC1 Expression in Models of Gastric Cancer. *Cancer Lett* **2012**, *321* (2), 128–136. https://doi.org/10.1016/j.canlet.2012.01.019.
- (39) Castillo-Ávila, W.; Piulats, J. M.; Garcia Del Muro, X.; Vidal, A.; Condom, E.; Casanovas, O.; Mora, J.; Ramon Germà, J.; Capellà, G.; Villanueva, A.; Viñals, F. Sunitinib Inhibits Tumor Growth and Synergizes with Cisplatin in Orthotopic Models of Cisplatin-Sensitive and Cisplatin-Resistant Human Testicular Germ Cell Tumors. *Clinical Cancer Research* **2009**, *15* (10), 3384–3395. https://doi.org/10.1158/1078-0432.CCR-08-2170.
- (40) Lopergolo, A.; Nicolini, V.; Favini, E.; Bo, L. D.; Tortoreto, M.; Cominetti, D.; Folini, M.; Perego, P.; Castiglioni, V.; Scanziani, E.; Borrello, M. G.; Zaffaroni, N.; Cassinelli, G.; Lanzi, C. Synergistic Cooperation between Sunitinib and Cisplatin Promotes Apoptotic Cell Death in Human Medullary Thyroid Cancer. *Journal of Clinical Endocrinology and Metabolism* 2014, 99 (2), 498–509. https://doi.org/10.1210/jc.2013-2574.
- (41) Arantes-Rodrigues, R.; Pinto-Leite, R.; Fidalgo-Gonçalves, L.; Palmeira, C.; Santos, L.; Colaço, A.; Oliveira, P. Synergistic Effect between Cisplatin and Sunitinib Malate on Human Urinary Bladder-Cancer Cell Lines. *Biomed Res Int* **2013**, *2013*. https://doi.org/10.1155/2013/791406.
- (42) Dhara, S. A Rapid Method for the Synthesis of Cis-[Pt(NH3)2Cl2]. *Indian J Chem* **1970**, 8, 193–194.
- (43) Brandon, R. J.; Dabrowiak, J. C. Synthesis, Characterization, and Properties of a Group of Platinum(Iv) Complexes. *J Med Chem* **1984**, *27* (7), 861–865. https://doi.org/10.1021/jm00373a009.
- (44) Tolan, D. A.; Abdel-Monem, Y. K.; El-Nagar, M. A. Anti-Tumor Platinum (IV) Complexes Bearing the Anti-Inflammatory Drug Naproxen in the Axial Position. *Appl Organomet Chem* **2019**, *33* (3). https://doi.org/10.1002/aoc.4763.
- (45) Sansook, S.; Ocasio, C. A.; Day, I. J.; Tizzard, G. J.; Coles, S. J.; Fedorov, O.; Bennett, J. M.; Elkins, J. M.; Spencer, J. Synthesis of Kinase Inhibitors Containing a Pentafluorosulfanyl Moiety. *Org Biomol Chem* **2017**, *15* (40), 8655–8660. https://doi.org/10.1039/c7ob02289a.
- (46) Beirne, D. F.; Dalla Via, M.; Velasco-Torrijos, T.; Montagner, D. Metal-Tyrosine Kinase Inhibitors: Targeted Metal-Drug Conjugates. *Coordination Chemistry Reviews*. Elsevier B.V. October 15, 2022. https://doi.org/10.1016/j.ccr.2022.214655.
- (47) Wang, Y.; Peng, C.; Wang, G.; Xu, Z.; Luo, Y.; Wang, J.; Zhu, W. Exploring Binding Mechanisms of VEGFR2 with Three Drugs Lenvatinib, Sorafenib, and Sunitinib by Molecular Dynamics Simulation and Free Energy Calculation. *Chem Biol Drug Des* **2019**, *93* (5), 934–948. https://doi.org/10.1111/cbdd.13493.

- (48) Wu, P.; Nielsen, T. E.; Clausen, M. H. FDA-Approved Small-Molecule Kinase Inhibitors. Trends Pharmacol Sci 2015, 36 (7), 422–439. https://doi.org/10.1016/j.tips.2015.04.005.
- (49) Argyros, O.; Karampelas, T.; Asvos, X.; Varela, A.; Sayyad, N.; Papakyriakou, A.; Davos, C. H.; Tzakos, A. G.; Fokas, D.; Tamvakopoulos, C. Peptide-Drug Conjugate Gnrh-Sunitinib Targets Angiogenesis Selectively at the Site of Action to Inhibit Tumor Growth. *Cancer Res* **2016**, *76* (5), 1181–1192. https://doi.org/10.1158/0008-5472.CAN-15-2138.
- (50) Moynihan, E.; Bassi, G.; Ruffini, A.; Panseri, S.; Montesi, M.; Velasco-Torrijos, T.; Montagner, D. Click Pt(IV)-Carbohydrates Pro-Drugs for Treatment of Osteosarcoma. *Front Chem* **2021**, *9*. https://doi.org/10.3389/fchem.2021.795997.
- (51) Moynihan, E.; Galiana-Cameo, M.; Sandri, M.; Ruffini, A.; Panseri, S.; Velasco-Torrijos, T.; Montesi, M.; Montagner, D. 2D and 3D Anticancer Properties of C2-Functionalised Glucosamine-Pt (IV) Prodrugs Based on Cisplatin Scaffold. Front Chem 2024, 12 (May), 1–11. https://doi.org/10.3389/fchem.2024.1388332.
- (52) Moynihan, E.; Panseri, S.; Bassi, G.; Rossi, A.; Campodoni, E.; Dempsey, E.; Montesi, M.; Velasco-Torrijos, T.; Montagner, D. Development of Novel Pt(IV)-Carbohydrate Derivatives as Targeted Anticancer Agents against Osteosarcoma. *Int J Mol Sci* **2023**, 24 (7). https://doi.org/10.3390/ijms24076028.
- (53) Marangon, E.; Buzzo, M.; Posocco, B.; Gagno, S.; Zanchetta, M.; Iacuzzi, V.; Poetto, A. S.; Guardascione, M.; Giodini, L.; Toffoli, G. A New High-Performance Liquid Chromatography—Tandem Mass Spectrometry Method for the Determination of Sunitinib and N-Desethyl Sunitinib in Human Plasma: Light-Induced Isomerism Overtaking towards Therapeutic Drug Monitoring in Clinical Routine. *J Pharm Biomed Anal* 2020, 179, 112949. https://doi.org/10.1016/j.jpba.2019.112949.
- (54) Prasad, M. Investigation of Z-E Isomerism in Sunitinib Anticancer Drug. **2014**, *3* (3), 1055–1058.
- (55) Posocco, B.; Buzzo, M.; Giodini, L.; Crotti, S.; D'Aronco, S.; Traldi, P.; Agostini, M.; Marangon, E.; Toffoli, G. Analytical Aspects of Sunitinib and Its Geometric Isomerism towards Therapeutic Drug Monitoring in Clinical Routine. *J Pharm Biomed Anal* **2018**, 160, 360–367. https://doi.org/10.1016/j.jpba.2018.08.013.
- (56) Matsunaga, N.; Kitahara, T.; Yamada, M.; Sato, K.; Kodama, Y.; Sasaki, H. The Influence of Light Sources on Sunitinib Measurements with Photoisomerization. *Biomedical Chromatography* **2019**, *33* (2), 99–101. https://doi.org/10.1002/bmc.4407.
- (57) Maafi, M.; Lee, L. Y. Actinometric and Φ-Order Photodegradation Properties of Anti-Cancer Sunitinib. J Pharm Biomed Anal 2015, 110, 34–41. https://doi.org/10.1016/j.jpba.2015.02.026.
- (58) Padervand, M.; Ghaffari, S.; Attar, H.; Nejad, M. M. Reverse Phase HPLC Determination of Sunitinib Malate Using UV Detector, Its Isomerisation Study, Method Development and Validation. *Journal of Analytical Chemistry* **2017**, *72* (5), 567–574. https://doi.org/10.1134/S1061934817050082.
- (59) Ngai, M. H.; So, C. L.; Sullivan, M. B.; Ho, H. K.; Chai, C. L. L. Photoinduced Isomerization and Hepatoxicities of Semaxanib, Sunitinib and Related 3-Substituted Indolin-2-Ones. *ChemMedChem* **2016**, *11* (1), 72–80. https://doi.org/10.1002/cmdc.201500475.

- (60) Rodamer, M.; Elsinghorst, P. W.; Kinzig, M.; Gütschow, M.; Sörgel, F. Development and Validation of a Liquid Chromatography/Tandem Mass Spectrometry Procedure for the Quantification of Sunitinib (SU11248) and Its Active Metabolite, N-Desethyl Sunitinib (SU12662), in Human Plasma: Application to an Explorative Study. *J Chromatogr B Analyt Technol Biomed Life Sci* **2011**, *879* (11–12), 695–706. https://doi.org/10.1016/j.jchromb.2011.02.006.
- (61) Gabano, E.; Zanellato, I.; Pinton, G.; Moro, L.; Ravera, M.; Osella, D. The Strange Case: The Unsymmetric Cisplatin-Based Pt(IV) Prodrug [Pt(CH3COO)CI2(NH3)2(OH)] Exhibits Higher Cytotoxic Activity with Respect to Its Symmetric Congeners Due to Carrier-Mediated Cellular Uptake. *Bioinorg Chem Appl* 2022, 2022. https://doi.org/10.1155/2022/3698391.
- (62) Kastner, A.; Poetsch, I.; Mayr, J.; Burda, J. V.; Roller, A.; Heffeter, P.; Keppler, B. K.; Kowol, C. R. A Dogma in Doubt: Hydrolysis of Equatorial Ligands of PtIV Complexes under Physiological Conditions. *Angewandte Chemie International Edition* 2019, 58 (22), 7464–7469. https://doi.org/10.1002/anie.201900682.
- (63) Zotti, G.; Berlin, A.; Vercelli, B. Electrochemistry of Conjugated Planar Anticancer Molecules: Irinotecan and Sunitinib. *Electrochim Acta* 2017, 231, 336–343. https://doi.org/10.1016/j.electacta.2017.02.043.
- (64) Liu, X.; Barth, M. C.; Cseh, K.; Kowol, C. R.; Jakupec, M. A.; Keppler, B. K.; Gibson, D.; Weigand, W. Oxoplatin-Based Pt(IV) Lipoate Complexes and Their Biological Activity. Chem Biodivers 2022, 19 (10). https://doi.org/10.1002/cbdv.202200695.
- (65) DiscoverX. *KinomeScan assay service*. https://www.discoverx.com/products-applications/kinase-solutions?gclid=EAlalQobChMIs3mrL2V\_gIVIM13Ch0RrAK8EAAYAiAAEgJEsPD\_BwER.J
- (66) Fazio, N.; Kulke, M.; Rosbrook, B.; Fernandez, K.; Raymond, E. Updated Efficacy and Safety Outcomes for Patients with Well-Differentiated Pancreatic Neuroendocrine Tumors Treated with Sunitinib. *Target Oncol* **2021**, *16* (1), 27–35. https://doi.org/10.1007/s11523-020-00784-0.
- (67) Oikawa, T.; Hitomi, J.; Kono, A.; Kaneko, E.; Yamaguchi, K. Frequent Expression of Genes for Receptor Tyrosine Kinases and Their Ligands in Human Pancreatic Cancer Cells; 1995; Vol. 18.
- (68) Carrato, A.; Swieboda-Sadlej, A.; Staszewska-Skurczynska, M.; Lim, R.; Roman, L.; Shparyk, Y.; Bondarenko, I.; Jonker, D. J.; Sun, Y.; De La Cruz, J. A.; Williams, J. A.; Korytowsky, B.; Christensen, J. G.; Lin, X.; Tursi, J. M.; Lechuga, M. J.; Van Cutsem, E. Fluorouracil, Leucovorin, and Irinotecan plus Either Sunitinib or Placebo in Metastatic Colorectal Cancer: A Randomized, Phase III Trial. *Journal of Clinical Oncology* 2013, 31 (10), 1341–1347. https://doi.org/10.1200/JCO.2012.45.1930.
- (69) Saltz, L. B.; Rosen, L. S.; Marshall, J. L.; Belt, R. J.; Hurwitz, H. I.; Eckhardt, S. G.; Bergsland, E. K.; Haller, D. G.; Lockhart, A. C.; Rocha Lima, C. M.; Huang, X.; DePrimo, S. E.; Chow-Maneval, E.; Chao, R. C.; Lenz, H. J. Phase II Trial of Sunitinib in Patients with Metastatic Colorectal Cancer after Failure of Standard Therapy. *Journal of Clinical Oncology* 2007, 25 (30), 4793–4799. https://doi.org/10.1200/JCO.2007.12.8637.
- (70) Shim, M.; Song, C.; Park, S.; Choi, S. K.; Cho, Y. M.; Kim, C. S.; Ahn, H. Prognostic Significance of Platelet-Derived Growth Factor Receptor-β Expression in Localized

- Clear Cell Renal Cell Carcinoma. *J Cancer Res Clin Oncol* **2015**, *141* (12), 2213–2220. https://doi.org/10.1007/s00432-015-2019-x.
- (71) Sun, C.; Li, H. L.; Chen, H. R.; Shi, M. L.; Liu, Q. H.; Pan, Z. Q.; Bai, J.; Zheng, J. N. Decreased Expression of CHIP Leads to Increased Angiogenesis via VEGF-VEGFR2 Pathway and Poor Prognosis in Human Renal Cell Carcinoma. *Sci Rep* **2015**, *5*. https://doi.org/10.1038/srep09774.
- (72) Huang, D.; Ding, Y.; Li, Y.; Luo, W. M.; Zhang, Z. F.; Snider, J.; VandenBeldt, K.; Qian, C. N.; Teh, B. T. Sunitinib Acts Primarily on Tumor Endothelium Rather than Tumor Cells to Inhibit the Growth of Renal Cell Carcinoma. *Cancer Res* **2010**, *70* (3), 1053–1062. https://doi.org/10.1158/0008-5472.CAN-09-3722.
- (73) Jensen, C.; Teng, Y. Is It Time to Start Transitioning From 2D to 3D Cell Culture? Frontiers in Molecular Biosciences. Frontiers Media S.A. March 6, 2020. https://doi.org/10.3389/fmolb.2020.00033.